High dynamic range land wavefield reconstruction from randomized acquisition

Iga Pawelec* **and Paul Sava***

**Colorado School of Mines,*

1500 Illinois St,

Golden, CO 80401

(March 14, 2023)

CWP-1017

Running head: **HDR wavefield reconstruction**

ABSTRACT

Compressive sensing (CS) is an alternative to regular Shannon sampling capable of capturing the same amount of information about seismic wavefields from much reduced measurements. It relies on randomized sampling patterns and a sparse data representation in a domain of interest to reconstruct the regularly sampled object. This technology applied to land seismic acquisition design promises to deliver the same data quality as a regular acquisition with fewer samples or superior data quality with the same number of samples. Compressive sensing is a strong contender for helping to overcome some of the challenges associated with land seismic data, providing the ability to affordably record the intricate wavefields propagating in the near surface without aliasing. Recording high-quality non-aliased wavefields can lead to significant improvements in the understanding of the near surface and in suppressing noise. However, near surface wave phenomena tend to propagate with low velocities and contain the majority of the source-generated energy, making the much weaker reflection signals barely discernible. This results in data that are rich in high wavenumber

content and have amplitudes of interest that span several orders of magnitude. When dealing with high dynamic range non-stationary data, the Fourier domain is not optimal for providing sparse representation - a necessary condition for successful application of compressive sensing. In contrast, a discrete complex wavelet transform can localize high energy features, has good directional selectivity, and is near-shift invariant. Combined, these properties allow complex wavelets to represent detail-rich wavefields with high dynamic range in a compact form which is essential for a sparsity-promoting reconstruction.

Another important ingredient of a successful CS data reconstruction is the choice of an appropriate sparsity-promoting algorithm. Since complex wavelets provide a multiscale signal representation, global approaches that simply rely on the distribution of high energy coefficients in the transform domain are not the best choice. To account for differences in coefficient energy distributions at different decomposition levels of the complex wavelet transform, we develop a scale- and orientation- dependent iterative soft thresholding scheme (IST) for reconstructing land wavefields. Our approach requires little parametrization, is easy to implement, and robust to reconstructed wavefield sampling grid and dynamic range. We test the developed soft thresholding scheme on different wavefields with randomly missing traces, and compare the data reconstructions to the spectral projected gradient solver and projection onto convex sets. We quantify the reconstructions by a direct comparison of Fourier coefficients between fully sampled and reconstructed wavefields. Taking log10 of Fourier coefficients prior to computing the quality metric de-emphasizes the importance of magnitude match while highlighting Fourier coefficient support accuracy which usually translates into good structural fidelity of reconstructed data. We find that our IST performs consistently among all examples, yielding high structural fidelity while performing gentle denoising.

INTRODUCTION

Land seismic data suffer from a number of quality issues, such as low signal-to-noise ratio, phase distortions, or environmental noise. The majority of these problems stem from the near surface noise (Regone, 1997) and can be addressed by acquiring non-aliased wavefields. However, achieving this goal following the classical sampling theorem (Shannon, 1948; Jerri, 1977) is prohibitively expensive due to the required trace density. The near surface often consists of loose soil and poorly consolidated sediments, giving rise to strong and slow surface waves, guided waves, and scattering noise, especially in presence of lateral heterogeneities (Stork, 2020). The waves traveling in the near surface are only sensitive to the upper 10s or 100s of meters and provide no information on the deeper structure and are considered noise for most imaging applications. However, it is recognized that high fidelity recording of the surface waves is valuable in building the near surface models and computing reliable static corrections (Socco et al., 2010; Krohn and Routh, 2017; Monk, 2020). The need to record non-aliased surface waves is thus twofold: 1) to constrain the near surface model and 2) to remove them from seismic records without compromising the significantly weaker reflections.

The sampling needed for regular non-aliased recording is dictated by the slowest phase velocity expected in the seismic record and the highest frequency present in that signal. Figures 1a and 1b show examples of densely sampled land records with their corresponding FK spectra in Figures 1d and 1e. Note that the strong energy associated with surface waves has phase velocities below 200 m/s and reaches frequencies of 50-60 Hz. In these scenarios, the regular sampling interval would have to be less than 2 m which is not feasible for large scale surveys: terrain obstacles and access restrictions often prevent placement of sources and/or receivers at desired locations. Stork (2023) argues that some locations for sources or receivers can be predicted as noisy and problematic prior to the survey, furthering the case for deliberate irregular acquisition. Enabled by recent

advances in nodal acquisition technology (Freed, 2008; Manning et al., 2018), compressive sensing (CS) emerges as a feasible methodology for acquiring data on an irregular grid and with smaller channel count than required for a regular survey, allowing for recovery of non-aliased wavefield on a regular grid as a post-acquisition step.

Developed in the signal processing community, CS is one possible solution to the problem of retaining the needed information about the signal of interest from reduced measurements. Early works by Candès et al. (2006a); Donoho (2006) establish the CS theoretical framework. There are two main elements to the CS approach: selection of sampling scheme that is as incoherent as possible with respect to the domain in which data are considered sparse (Candès and Romberg, 2007; Candès and Wakin, 2008), and the appropriate choice of reconstruction strategy.

Different sampling schemes were considered for geophysical applications. Hennenfent and Herrmann (2008) show that for localized transforms such as curvelet transform it may be beneficial to constrain randomized sampling with the maximum gap size, ensuring that there are no regions containing only zeros within the entire operator support. Naghizadeh and Sacchi (2010) investigate multidimensional sampling operators in the Fourier domain and conclude that randomly sampled multidimensional data should only suffer from a minor spectral distortion. Jiang et al. (2018) design a CS field trial defining their source and receiver sampling locations on regularly indexed grid accounting for access restrictions and implementing gap size control while minimizing aliased energy in the sparse domain. Though the benefits of CS for seismic data acquisition have been demonstrated (Mosher et al., 2017; Jiang et al., 2019; Blymyer et al., 2021), finding the optimal reconstruction strategy for specific sampling scheme and sparse domain remains an open research area.

One of the most popular choices for a sparse domain in seismic data acquisition and reconstruction is the Fourier domain. Liu and Sacchi (2004) introduce minimum weighted norm interpolation

with spectral weights derived directly from data and adjusted iteratively. Trad (2009) extend the reconstruction approach to five dimensions. Though memory-consuming, such an extension is particularly favorable for seismic data sparse recovery: 5D objects tend to be more sparse than 2D or even 3D objects. Because wavefields usually vary the fastest along time, and less rapidly over space, adding spatial dimensions (sources and receivers) introduces reciprocal information, contributing to the sparsity of the entire object. For the same reason, successful reconstruction of 2D gathers tends to be more challenging, particularly on land, where amplitudes can vary by several orders of magnitude over short distances. The gathers shown in Figures 1a and 1b are examples of 2D land wavefields showcasing that particular feature which we highlight by using a semi-logarithmic color normalization available in *matplotlib* (Hunter, 2007). The strongest energy is concentrated in the source region and can be four orders of magnitude higher than the energy 200 m away. For contrast, we also show a window from a synthetic gather in Figure 1c. Note that, though the wavefield is intricate, the amplitude variability over distance is not significant. High dynamic range objects such as raw land seismic wavefields containing near offsets are not well-approximated as sparse in the Fourier domain (Pawelec et al., 2021). The FK spectra in Figures 1d and 1e illustrate why: rapid energy decay introduces large number of non-zero Fourier coefficients, and setting these coefficients to zero leads to substantial signal distortions. As a result, Fourier-based reconstructions require data windowing, range compression, or working on a single frequency slice at a time. The discrete complex wavelet transform ($\mathbb{C}$WT) does not suffer from this problem. Complex wavelets are localized in time and space and have directional sensitivity (6 directions in 2D and 28 directions in 3D). With linear computation time and only 2^D redundancy for $D-$dimensional signals, complex wavelets are particularly attractive for representing and analyzing non-stationary signals. In particular, $\mathbb{C}$WT found applications in denoising (Julayusefi et al., 2012; Peng et al., 2014; Yu et al., 2017, 2022) and discontinuity detection (Liang et al., 2019), but its use for data reconstruction is

not well-studied despite indications that it shows promise, outperforming some popular contestants such as curvelets (Li et al., 2014; Pawelec et al., 2021).

Since complex wavelets can sparsely represent high dynamic range wavefields, they allow for reconstructing detail-rich land records without windowing or amplitude processing (i.e. gain or normalization). However, reconstruction success strongly depends on the reconstruction approach. The basis pursuit with projected spectral gradient (SPGL1) method (van den Berg and Friedlander, 2009, 2011) is a common choice for solving sparsity-promoting regularization problems because it is readily available and can handle complex numbers. In seismic interpolation problems, a popular data reconstruction strategy is projection onto convex sets (POCS) due to its ease of implementation and relatively straightforward parametrization (Abma and Kabir, 2006; Gao et al., 2013). We show that yet another approach, an iterative soft thresholding (IST)(Donoho, 1995; Daubechies et al., 2004), can match or better the reconstructions obtained from SPGL1 and POCS, as demonstrated by Fourier domain SNR. Though iterative soft thresholding with wavelets, often referred to as 'wavelet shrinkage' (Donoho et al., 1995), has been successfully used in image restoration problems, we are not aware of its application to seismic data reconstruction. Our main contribution is developing a strategy for scale- and orientation-dependent thresholding that is inspired by the link of the mixed norm minimization problem with ℓ_1 constraint to the maximum *a posteriori* estimate with a Laplacian prior (Alliney and Ruzinsky, 1994; Tibshirani, 1996; Figueiredo et al., 2007). The only parameter required for the initial threshold estimation is the noise standard deviation σ_n. We show that this parameter can be estimated directly from data, yielding threshold values that converge on a good reconstruction. As a result, IST is easy to use and implement and yields high-quality reconstructions. Furthermore, if one adjusts the stopping criterion appropriately, IST can also be used as a denoising tool.

This manuscript begins with a brief review of the basic properties of the complex wavelet trans-

form and introduces the intuition behind correspondence of scales and orientations and Fourier frequency-wavenumber bands. Next, we discuss the compressive sensing framework and the iterative thresholding approach. We then show reconstructions for randomly decimated wavefields with 50% missing traces which highlight the favorable qualities of soft thresholding and POCS. Finally, we summarize our findings and conclude that iterative soft thresholding is the optimal complex-wavelet domain reconstruction strategy, easy to implement, and capable of reconstructing structurally-consistent wavefields.

COMPLEX WAVELET TRANSFORM

The discrete complex wavelet transform ($\mathbb{C}$WT) extends the real wavelet transform by introducing several desirable qualities absent from a critically sampled real wavelet transform (Selesnick et al., 2005). First, unlike real wavelets that exhibit oscillatory behavior around singularities, the magnitude of $\mathbb{C}$WT is consistently high around such features, allowing for more intuitive coefficient interpretation and feature identification. Second, $\mathbb{C}$WT is near-shift invariant:, i.e., small signal shift causes only a minor change in coefficient magnitude with a near-linear phase encoding of the shift amount. Thus, this property limits the number of possible coefficient patterns introduced for example by shifting the sampling matrix, yielding more predictable reconstruction results. Third, complex wavelets in two and more dimensions offer enhanced directional selectivity, avoiding the 'mixing' of directions characteristic of the real transform (e.g. its inability to distinguish between $\pm 45^{\circ}$). Finally, $\mathbb{C}$WT is less sensitive to coefficient aliasing that results from transform implementation via an imperfect filter bank (filters do not completely attenuate signal's spectral content outside of filter's pass band).

While $\mathbb{C}$WT is a redundant transform, the redundancy factor does not depend on scale and is 2^m

for m-D signals (Kingsbury, 2001; Selesnick et al., 2005). Similarly to the Fourier transform, when $\mathbb{C}$WT is used for analyzing real-valued signals, coefficient symmetries can be exploited, allowing for memory savings with the right transform implementation. We use $\mathbb{C}$WT implementation via dual-tree filter bank of real wavelet filters, with the two tree branches providing real and imaginary parts of complex coefficients. The filters used for $\mathbb{C}$WT must meet stringent design criteria including perfect reconstruction and jointly yielding an approximately analytic transform. Kingsbury (2001) and Selesnick (2002) provide detailed requirements.

The orientations in the complex wavelet transform are related to the idealized Fourier domain support of each wavelet. The common interpretation of these orientations in 2D is related to features oriented at specific angles: $\pm 15°$, $\pm 45°$, and $\pm 75°$. However, while such interpretation may be helpful for natural images, it gives little insight for seismic data with spatial and temporal dimensions. Thus, it is helpful to represent complex wavelet coefficients on their idealized Fourier domain support. While the coefficients at specific scale and orientation are supposed to represent signal features from specific octave band, they can also contain some frequency and wavenumber information outside of that band because wavelets are not perfectly analytical and filters implementing the transform not perfect. Despite that, showing $\mathbb{C}$WT coefficients in the Fourier space offers valuable insight. Figure 2 visualizes coefficient magnitudes for a transform of the wavefield from Figure 1b before and after random trace decimation. The correspondence of $\mathbb{C}$WT's angles to more natural phase velocities is not simply that steeply dipping events correspond to high angles. Instead, the highest concentration of complex wavelet coefficients corresponding to a particular dipping event depends on spatial and temporal sampling. Since wavefields are frequently oversampled in time, one may want to resample seismic data such that all sampling dimensions (space and time) have usable information up to their respective Nyquist wavenumber or frequency, allowing for better representation of specific wavefield features in the complex wavelet domain.

Note that complex wavelet coefficients in Figure 2 are displayed on logarithmic scale. The common wisdom that high energy coefficients correspond to high energy events holds true. Trace decimation introduces artifacts, but rather than being spread randomly throughout the whole domain, these effects are fairly localized. At the finest scale, we see high energy coefficients introduced for high wavenumber, low frequency quadrant (top left corner marked by a yellow box). Figures 2c and 2d are a zoom-in at the scale and orientation marked by the box. Coefficients are plotted on the same color scale, showing that after random trace decimation, missing trace magnitudes are weakened, while the magnitudes representing the remaining traces are strengthened. The strengthening is likely because gaps in the wavefield are perceived as singularities. This furthers the case for soft thresholding: we would like to rebuild coefficient magnitudes inside gaps while weakening them for the available data. A sparsity promoting algorithm that simply seeks to preserve the high energy coefficients in the transform domain while disregarding weak coefficients as noise is likely to reinforce data discontinuities. By driving these weak energy coefficients corresponding to gap locations to zero we may ultimately prevent the recovery of the missing information. One way to counteract that is to introduce a low resolution initial estimate (Gorodnitsky and Rao, 1997).

COMPRESSIVE SENSING

Compressive sensing is a sampling / sensing paradigm allowing for recovery of signals from incomplete measurements (Candès et al., 2006a; Candès and Tao, 2006). The key assumption is that the target signal is or can be approximated as sparse in some representation, and that it is sampled in the right way. Sparsity means that the signal's information content can be expressed in a concise form, for example by encoding locations and values of large wavelet coefficients in image compression problems (Taubman, 2002). The concept of 'right sampling' is related to the relationship between the sensing basis - 'the data domain' in the case of seismic acquisition - and the representation basis

- data representation in the sparse domain. Formally, that relationship is described by coherence μ

$$\mu(\mathbf{\Phi}, \mathbf{\Psi}) = \sqrt{n} \cdot \max_{1 \leq k,j \leq n} |\langle \phi_k, \psi_j \rangle|, \tag{1}$$

where ϕ and ψ represent basis functions from sensing and representation basis, respectively. When the two bases have correlated elements, the coherence is large. In general, it is desirable to find the pairing of bases for which the coherence is as small as possible, i.e., the bases that do not have correlated elements. The combination of spikes in the physical domain and the Fourier basis has maximal incoherence, hence one of the reasons for its popularity. Wavelet transforms are local; when used as a sparse basis for signals acquired with random spikes, the sampling artifacts should not spread through the whole domain. It leads to an interesting conundrum for compressive sensing of seismic signals. From a practical point of view, the non-uniform sampling (i.e., either placing the receiver and/or source on the grid or skipping the sampling location altogether) is the easiest to achieve for seismic acquisition. Additional constraints can be placed on the geometry, for example to limit the gap size for the benefit of reconstruction strategies or to account for natural obstacles. For this type of sampling, Fourier representation seems like a natural choice. However, if the goal is to recover raw high dynamic range records, the Fourier basis cannot sufficiently sparsify such signals. Complex wavelets are less ideal from the coherency point of view, but provide significantly sparser wavefield representation, making them a viable alternative to the Fourier basis.

Once the sensing and sparse bases are selected, the underlying signal can be recovered by a sparsity-promoting algorithm. There are many possible choices that fall into at least two categories: greedy pursuits that approximate signals looking for locally optimal representations one coefficient at a time (Tropp, 2004; Tropp and Gilbert, 2007; Needell and Tropp, 2009) and convex relaxation methods that solve a convex optimization problem that approximates the target signal (Daubechies

et al., 2004; Candès et al., 2006b; van den Berg and Friedlander, 2009, 2011). The convex optimization usually uses the ℓ_1 norm to enforce the sparsity constraint and is formulated as

$$\min \|\boldsymbol{\alpha}\|_1 \text{ s. t. } \|\mathbf{d} - \mathbf{S}\boldsymbol{\Psi}^H\boldsymbol{\alpha}\|_2^2 \leq \epsilon, \tag{2}$$

where $\boldsymbol{\alpha}$ is a coefficient vector in the sparse domain, $\mathbf{S}$ is the sampling matrix, $\boldsymbol{\Psi}$ is the sparsifying transform, and $\mathbf{d}$ is the recorded data. Basis pursuit and iterative soft thresholding fall into this latter family of algorithms. Projection onto convex sets (POCS) falls into the greedy pursuit family.

ITERATIVE SOFT THRESHOLDING

Wavelet thresholding, sometimes referred to as 'shrinkage' (Donoho et al., 1995; Chambolle et al., 1998) is a well-established technique used for image restoration (Donoho, 1995; Bioucas-Dias and Figueiredo, 2007; Raj and Venkateswarlu, 2012) and aims to recover a high-quality image from degraded samples, with degradation that can be purely due to noise, or blurring, or both. Iterative soft thresholding also arises naturally as a way of solving a mixed norm minimization problem:

$$\min_{\boldsymbol{\alpha}} \|\mathbf{d} - \mathbf{G}\boldsymbol{\alpha}\|_2^2 + \lambda\|\boldsymbol{\alpha}\|_1. \tag{3}$$

In the context of complex wavelet seismic data reconstruction, $\mathbf{G} = \mathbf{S}\boldsymbol{\Psi}^H$, with sampling matrix $\mathbf{S}$, and inverse complex wavelet transform $\boldsymbol{\Psi}^H$, while $\boldsymbol{\alpha}$ represents the complex wavelet coefficients of fully sampled wavefield. λ is the regularization parameter that in the IST fulfills the role of threshold. The algorithm iterations involve matrix-vector multiplications with $\mathbf{G}$ and $\mathbf{G}^H$ followed by the shrinkage / soft threshold step (Chambolle et al., 1998; Figueiredo and Nowak, 2003; Beck and Teboulle, 2009):

$$\boldsymbol{\alpha}_{k+1} = \mathcal{T}_{\lambda t}\Big(\boldsymbol{\alpha}_k - 2t\mathbf{G}^H(\mathbf{G}\boldsymbol{\alpha}_k - \mathbf{d})\Big), \tag{4}$$

where t is the step size and the soft thresholding operator is defined as

$$\mathcal{T}_\lambda(\boldsymbol{\alpha})_i = (|\alpha_i| - \lambda)_+ \mathrm{sgn}(\alpha_i) = \begin{cases} \alpha_i + \lambda & \text{for } \alpha_i \leq -\lambda \\ 0 & \text{for } |\alpha_i| < \lambda \\ \alpha_i - \lambda & \text{for } \alpha_i \geq \lambda \end{cases}, \tag{5}$$

with the threshold λ. Note that this operator is defined for real-valued functions, however, the extension to complex numbers is straightforward. Let $\alpha_i = re^{j\theta}$. Then, the complex thresholding operator is simply $\mathcal{T}_\lambda(re^{j\theta}) = \mathcal{T}_\lambda(r)e^{j\theta}$ (Daubechies et al., 2004).

Determining thresholds appropriate for a specific problem can be a challenge. The most common approach is to find a global threshold, or in other words, a single threshold value that is applied to all coefficients. While performance of such an approach is reasonable if the noise is stationary, the results can quickly deteriorate when the noise power varies from sample to sample (Lo and Selesnick, 2006). For instance, signal-to-noise ratio for seismic data depends on offset, and the disturbance introduced by irregular sampling does not affect all complex wavelet decomposition coefficients equally (Figure 2b). Therefore, introducing scale- and orientation-dependent thresholds has merit because it accounts for different coefficient energy levels among transform scales and orientations. The question remains: how does one determine the appropriate thresholds? The answer lies in the link of the mixed norm optimization problem from equation 3 to the probabilistic framework (Alliney and Ruzinsky, 1994; Tibshirani, 1996; Figueiredo et al., 2007). From the Bayesian perspective, one can view equation 3 as a maximum *a posteriori* solution to finding $\boldsymbol{\alpha}$ from noisy

observations

$$\mathbf{d} = \mathbf{G}\boldsymbol{\alpha} + \mathbf{n}, \tag{6}$$

where the noise $\mathbf{n}$ is assumed to be Gaussian and white with variance σ_n, and $\boldsymbol{\alpha}$ belongs to a Laplace distribution. Under these assumptions, Lo and Selesnick (2006) suggest the following threshold definition

$$\lambda = \frac{\sqrt{2}\sigma_n^2}{\sigma_w}, \tag{7}$$

where σ_n is the standard deviation of the noise and σ_w is scale- and orientation-dependent standard deviation for the wavelets coefficients with a zero-mean Laplace distribution (Selesnick, 2009). Chang et al. (2000) advocate for a similar threshold but without $\sqrt{2}$ factor, providing full derivation and proving its near-optimality yielding denoising results within 5% mean squared error of the best soft thresholding benchmark. Although originally intended for natural image denoising, $\lambda = \frac{\sigma_n^2}{\sigma_w}$ is well-suited for seismic data reconstruction within iterative soft thresholding framework, provided that parameters σ_w and σ_n are selected appropriately. As suggested by Selesnick (2009), σ_w can be estimated as $\widehat{\sigma}_w = \sqrt{\max(\mathbb{E}[|\alpha|^2] - \sigma_n^2), 0}$, with α representing noisy wavelet coefficients at specific scale and orientation. The noise level σ_n can be estimated as median absolute deviation (MAD):

$$\widehat{\sigma}_n = k \cdot 1.4826 \cdot \mathrm{median}(|\alpha_i - \tilde{\alpha}|), \tag{8}$$

where $\tilde{\alpha}$ is the median of wavelet coefficients at specific scale and k is the empirically selected integer scaling factor. MAD is a robust statistical estimator and a popular choice when the noise is unknown (Donoho et al., 1995). A numerical constant of 1.4826 is related to the Gaussian distribution assumed for the noise. Since the imprint of sampling in the complex wavelet domain is the smallest for the coarsest scale, we recommend using the coarsest available scale with all orientations to obtain the value of $\widehat{\sigma}_n$, as in examples shown here. The choice of k depends on the level of data

decimation and the amplitude of events surrounding the gap. We find that values of k greater than 10 are required when there are substantial gaps in high amplitude features.

DATA RECONSTRUCTION EXAMPLES

To assess the performance of complex wavelet domain reconstruction, we randomly decimate 50% of the traces for wavefields shown in Figure 1. The three wavefields are used to avoid drawing conclusions from potentially biased results. We opt against introducing gap size control in this instance to better understand what the reconstruction limitations are. Note that the Fourier spectra of the tested wavefields indicate that they are critically sampled or suffer from minor aliasing. This is an important point because we might suffer potential information loss, particularly if significant gaps happen to fall in the near offset region where the energy concentration is high and events steeply dipping.

Each wavefield has the same number of samples in time and space and therefore the gap location indices are also the same in each scenario. The peak amplitude is 1 in all cases, but the minimum non-zero amplitude differs and is $1.48 \cdot 10^{-10}$, $4.86 \cdot 10^{-11}$, and $1.53 \cdot 10^{-8}$, respectively, clearly showing that wavefields have different dynamic ranges which impacts the reconstruction. Recall that highest energy wavelet coefficients correspond to high energy concentrations in data - however, there is also sampling noise resulting in relatively high coefficients in some places and near zero coefficients in others. The reconstructions should, ideally, start with the strong events and progressively stretch towards the low amplitude events while reducing sampling imprint on data. The bigger range of data to be reconstructed, the more iterations with high initial thresholds the reconstruction may need to restore events of interest.

The large dynamic range of the wavefields is also the reason to opt for Fourier domain rather

than data domain quality assessment. Any single number describing pixel-by-pixel differences between two objects can be misleading and counter-intuitive to human observer's perception, especially when large distortions or gaps are introduced (Eskicioglu and Fisher, 1995). That assessment is further compromised when both high and low amplitude features of an object are important. To partially avoid these pitfalls, we compute signal-to-noise ratios (SNR) in the Fourier domain for the original Fourier coefficients and for logarithmic transformation of these coefficients. First, the features of any specific trace are spread through Fourier domain, avoiding bias introduced by near-zero reconstruction difference where data are available and the large but often high frequency, high wavenumber differences where traces were missing. Second, taking the logarithm of Fourier coefficients magnitude before computing SNR helps to emphasize the coefficient structure, which is important for accurate representation of slopes in data.

Figure 3 shows reconstructions with basis pursuit, iterative soft thresholding, and projection onto convex sets in rows 1, 2, and 3, with their respective Fourier SNRs. The most visually striking difference is for the synthetic wavefield: the basis pursuit approach leaves many gaps unfilled or partially unfilled while both soft thresholding and POCS are able to overcome most of these gaps. A glance at data differences between original fully sampled wavefields and their reconstructions in Figure 4 shows that POCS is the most successful in restoring amplitude, while phase is consistent and reliable in both reconstructions. Interestingly, one gap that still remains in data is partially filled, depending on amplitude, wavelength and orientation of the events surrounding it. That is related to the preferential treatment of some orientations by the complex wavelet transform: for a circularly symmetric object, coefficients encoding some angles are not as strong as coefficients encoding other angles, leading to an unfortunate reconstruction artifacts (partially unfilled gap) when wavefield features happen to align with orientations represented by weaker energy coefficients.

The differences in reconstructions of land wavefields are more difficult to spot, partially due to

the logarithmic scale spanning six orders of magnitude necessary to make all events visible. The wavefield in Figure 1b is missing near offset information from the decimated data, causing the reconstruction in that region to be relatively difficult, particularly within the first 0.3 s. The basis pursuit additionally suffers from discontinuities in the reconstructed first arrival that thresholding methods manage to avoid.

One important advantage of the soft thresholding approach over POCS is that there is no requirement to perfectly match the original data to achieve the reconstruction: since both original traces and missing traces are reconstructed at the same time, one can decide on what level of original data fitting is desirable - the same is also true for basis pursuit with denoising. Here, we show iterative soft thresholding with a minor denoising that can be depicted on data differences in Figure 4. Denoising operations primarily target both coherent and incoherent high wavenumber events. Specifically for POCS, the original traces are re-injected at each iteration. While re-injection might be desirable when data are high quality, such an operation can be problematic in more noisy scenarios, resulting in reconstructing noise rather than signal inside gaps.

CONCLUSIONS

Complex wavelet domain thresholding techniques are successful in restoring land seismic wavefields with randomly decimated traces. Owing to the localized nature of the transform, both high and low amplitude events can be captured in a relatively sparse representation, allowing for accurate reconstructions of these features without the need for data windowing or amplitude processing. Both iterative soft thresholding and projection onto convex sets with support-based thresholding functions yield superior results to the basis pursuit with projected spectral gradient.

The success of soft thresholding relies on the scale- and orientation-based threshold definitions.

These thresholds are estimated directly from the decimated data, with the noise parameter computed using directional coefficients in the coarsest scale and multiplied by an integer constant. The choice of constant depends on the degree of data decimation, especially if gaps are located around strong events. We find that $k = 5$ is a good choice for data with less amplitude variation, such as Figure 1c, or when gaps are not concentrated around near offsets, like in Figure 1a, but $k = 40$ is needed to try and restore missing near offset information, particularly since 98.7% of the recorded shot energy is contained in $(-20, 20)$ m offset range. Soft thresholding has a natural termination point when the desired data residual is reached, making such an operation an attractive approach for denoising while reconstructing. Though POCS yields improved amplitude fidelity in the presented synthetic case, IST has consistently the highest SNR for log-compressed Fourier coefficients which indicates a better overall structural fidelity of the IST-reconstructed wavefields. Thanks to the provided recipe for finding σ_n and σ_w, our IST approach requires little user input and testing, making it fast and easy to use.

Projection onto convex sets also yields satisfactory reconstructions but needs more customization to select optimal bounds for starting and ending thresholding points as well as for the thresholds progression. For land wavefields, exponential thresholding scheme proves the best while the synthetic example benefits from linear step progression with a degree of Gaussian smoothing in the first few iterations. POCS is a good choice for reconstructing high quality data, but because the original unaltered traces are re-injected at each POCS iteration, the denoising effect cannot be achieved, affecting the reconstruction.

REFERENCES

Abma, R., and N. Kabir, 2006, 3D interpolation of irregular data with a POCS algorithm: Geophysics, **71**, E91–E97.

Alliney, S., and S. Ruzinsky, 1994, An algorithm for the minimization of mixed l/sub 1/ and l/sub 2/ norms with application to Bayesian estimation: IEEE Transactions on Signal Processing, **42**, 618–627.

Beck, A., and M. Teboulle, 2009, A fast iterative shrinkage-thresholding algorithm for linear inverse problems: SIAM Journal on Imaging Sciences, **2**, 183–202.

Bioucas-Dias, J., and M. Figueiredo, 2007, A new TwIST: two-step iterative shrinkage/thresholding algorithms for image restoration: IEEE Transactions on Image Processing, **16**, 2992–3004.

Blymyer, D., K. Koster, and G. Warren, 2021, A 108km2 Compressive Sensing Processing Trial: First International Meeting for Applied Geoscience & Energy Expanded Abstracts, Society of Exploration Geophysicists, 2630–2634.

Candès, E., and J. Romberg, 2007, Sparsity and incoherence in compressive sampling: Inverse Problems, **23**, 969–985.

Candès, E. J., J. Romberg, and T. Tao, 2006a, Robust uncertainty principles: exact signal reconstruction from highly incomplete frequency information: IEEE Transactions on Information Theory, **52**, 489–509.

Candès, E. J., J. K. Romberg, and T. Tao, 2006b, Stable signal recovery from incomplete and inaccurate measurements: Communications on Pure and Applied Mathematics, **59**, 1207–1223.

Candès, E. J., and T. Tao, 2006, Near-optimal signal recovery from random projections: universal encoding strategies?: IEEE Transactions on Information Theory, **52**, 5406–5425.

Candès, E. J., and M. B. Wakin, 2008, An Introduction To Compressive Sampling: IEEE Signal Processing Magazine, **25**, 21–30.

Chambolle, A., R. De Vore, Nam-Yong Lee, and B. Lucier, 1998, Nonlinear wavelet image processing: variational problems, compression, and noise removal through wavelet shrinkage: IEEE Transactions on Image Processing, **7**, 319–335.

Chang, S., Bin Yu, and M. Vetterli, 2000, Adaptive wavelet thresholding for image denoising and compression: IEEE Transactions on Image Processing, **9**, 1532–1546.

Daubechies, I., M. Defrise, and C. De Mol, 2004, An iterative thresholding algorithm for linear inverse problems with a sparsity constraint: Communications on Pure and Applied Mathematics, **57**, 1413–1457.

Donoho, D., 1995, De-noising by soft-thresholding: IEEE Transactions on Information Theory, **41**, 613–627.

Donoho, D. L., 2006, Compressed sensing: IEEE Transactions on Information Theory, **52**, 1289–1306.

Donoho, D. L., I. M. Johnstone, G. Kerkyacharian, and D. Picard, 1995, Wavelet Shrinkage: Asymptopia?: Journal of the Royal Statistical Society: Series B (Methodological), **57**, 301–337.

Eskicioglu, A. M., and P. S. Fisher, 1995, Image quality measures and their performance: IEEE Transactions on Communications, **43**, 2959–2965.

Figueiredo, M., and R. Nowak, 2003, An EM algorithm for wavelet-based image restoration: IEEE Transactions on Image Processing, **12**, 906–916.

Figueiredo, M. A., R. D. Nowak, and S. J. Wright, 2007, Gradient projection for sparse reconstruction: application to compressed sensing and other inverse problems: IEEE Journal of selected topics in signal processing, **1**, 586–597.

Freed, D., 2008, Cable-free nodes: The next generation land seismic system: The Leading Edge, **27**, 878–881.

Gao, J., A. Stanton, M. Naghizadeh, M. D. Sacchi, and X. Chen, 2013, Convergence improvement

and noise attenuation considerations for beyond alias projection onto convex sets reconstruction: Geophysical Prospecting, **61**, 138–151.

Gorodnitsky, I. F., and B. D. Rao, 1997, Sparse signal reconstruction from limited data using FOCUSS: A re-weighted minimum norm algorithm: IEEE Transactions on Signal Processing, **45**, 600–616.

Hennenfent, G., and F. J. Herrmann, 2008, Simply denoise: Wavefield reconstruction via jittered undersampling: Geophysics, **73**, V19–V28.

Hunter, J. D., 2007, Matplotlib: A 2D Graphics Environment: Computing in Science & Engineering, **9**, 90–95.

Jerri, A., 1977, The Shannon sampling theorem—Its various extensions and applications: A tutorial review: Proceedings of the IEEE, **65**, 1565–1596.

Jiang, T., P. Eick, Y. Jiang, T. Li, H. Hao, W. Chu, R. Holt, D. Blymyer, K. Koster, and D. Enns, 2019, Compressive sensing seismic processing tests on a high density blended land data set: SEG Technical Program Expanded Abstracts 2019, Society of Exploration Geophysicists, 4505–4509.

Jiang, T., Y. Jiang, D. Clark, R. Gray, and D. Brost, 2018, A compressive seismic field trial and reconstruction test using regular indexing: SEG Technical Program Expanded Abstracts, Society of Exploration Geophysicists, 86–90.

Julayusefi, M., A. R. Goudarzi, R. H. Bovanloo, and M. Shamounzadeh, 2012, Application of the 2-D dual-tree CWT as an image processing technique to attenuate remnant random noise of GPR signals.: International Geophysical Conference and Oil & Gas Exhibition, Istanbul, Turkey, 17-19 September 2012, Society of Exploration Geophysicists and The Chamber of Geophysical Engineers of Turkey, 1–4.

Kingsbury, N., 2001, Complex wavelets for shift invariant analysis and filtering of signals: Applied and Computational Harmonic Analysis, **10**, 234–253.

Krohn, C. E., and P. S. Routh, 2017, Exploiting surface consistency for surface-wave characterization and mitigation—Part 1: Theory and 2D examples: Geophysics, **82**, V21–V37.

Li, H., W. Yang, and X. Yong, 2014, Sparse reconstruction of 3D stochastic trace missing seismic data: Beijing 2014 International Geophysical Conference & Exposition, Beijing, China, 21-24 April 2014, Society of Exploration Geophysicists and Chinese Petroleum Society, 288–291.

Liang, Y., Z. Wang, X. Li, Z. Gao, Y. Xu, S. Zhang, and Y. Cai, 2019, Seismic discontinuous detection using dual-tree complex wavelet transform: 81st EAGE Conference and Exhibition 2019, European Association of Geoscientists & Engineers, 1–5.

Liu, B., and M. D. Sacchi, 2004, Minimum weighted norm interpolation of seismic records: Geophysics, **69**, 1560–1568.

Lo, W. Y., and I. W. Selesnick, 2006, Wavelet-domain soft-thresholding for non-stationary noise: 2006 International Conference on Image Processing, IEEE, 1441–1444.

Manning, T., C. Brooks, A. Ourabah, M. Popham, D. Ablyazina, V. Zhuzhel, E. Holst, and N. Goujon, 2018, The case for a nimble node, towards a new land seismic receiver system with unlimited channels, *in* SEG Technical Program Expanded Abstracts 2018: Society of Exploration Geophysicists, 21–25.

Monk, D. J., 2020, Survey design and seismic acquisition for land, marine, and in-between in light of new technology and techniques: Society of Exploration Geophysicists.

Mosher, C. C., C. Li, F. D. Janiszewski, L. S. Williams, T. C. Carey, and Y. Ji, 2017, Operational deployment of compressive sensing systems for seismic data acquisition: The Leading Edge, **36**, 661–669.

Naghizadeh, M., and M. D. Sacchi, 2010, On sampling functions and Fourier reconstruction methods: Geophysics, **75**, WB137–WB151.

Needell, D., and J. A. Tropp, 2009, CoSaMP: Iterative signal recovery from incomplete and inaccu-

rate samples: Applied and Computational Harmonic Analysis, **26**, 301–321.

Pawelec, I., M. Wakin, and P. Sava, 2021, Missing trace reconstruction for 2D land seismic data with randomized sparse sampling: Geophysics, **86**, P25–P36.

Peng, C., H. Jin, and P. Wang, 2014, Noise attenuation for multi-sensor streamer data via cooperative de-noising: Society of Exploration Geophysicists International Exposition and 84th Annual Meeting SEG 2014, 1878–1882.

Raj, V. N. P., and T. Venkateswarlu, 2012, Denoising of medical images using dual tree complex wavelet transform: Procedia Technology, **4**, 238–244.

Regone, C. J., 1997, Measurement and identification of 3-D coherent noise generated from irregular surface, *in* Carbonate seismology: Society of Exploration Geophysicists, 11, 281–306.

Selesnick, I., 2009, A Derivation of the Soft-Thresholding Function: Polytechnic Institute of New York University (lecture notes), 1–9.

Selesnick, I., R. Baraniuk, and N. Kingsbury, 2005, The dual-tree complex wavelet transform: IEEE Signal Processing Magazine, **22**, 123–151.

Selesnick, I. W., 2002, The design of approximate Hilbert transform pairs of wavelet bases: IEEE Transactions on Signal Processing, **50**, 1144–1152.

Shannon, C. E., 1948, A mathematical theory of communication: Bell System Technical Journal, **27**, 379–423.

Socco, L. V., D. Boiero, S. Foti, M. Maraschini, C. Piatti, P. Bergamo, F. Garofalo, M. Pastori, and G. D. Molino, 2010, Surface wave analysis for S-wave static correction computation: Society of Exploration Geophysicists International Exposition and 80th Annual Meeting 2010, SEG 2010, 1929–1933.

Stork, C., 2020, How does the thin near surface of the earth produce 10–100 times more noise on land seismic data than on marine data?: First Break, **38**, 67–75.

———, 2023, Using 'Noise-Corrected OVT Fold' to optimise land seismic acquisition risk, costs, and quality: First Break, **41**, 45–49.

Taubman, D. S., 2002, JPEG2000: Image compression fundamentals, standards and practice: Journal of Electronic Imaging, **11**, 286.

Tibshirani, R., 1996, Regression shrinkage and selection via the lasso: Journal of the Royal Statistical Society: Series B (Methodological), **58**, 267–288.

Trad, D., 2009, Five-dimensional interpolation: Recovering from acquisition constraints: Geophysics, **74**, V123–V132.

Tropp, J. A., 2004, Greed is good: algorithmic results for sparse approximation: IEEE Transactions on Information Theory, **50**, 2231–2242.

Tropp, J. A., and A. C. Gilbert, 2007, Signal recovery from random measurements via orthogonal matching pursuit: IEEE Transactions on Information Theory, **53**, 4655–4666.

van den Berg, E., and M. P. Friedlander, 2009, Probing the Pareto frontier for basis pursuit solutions: SIAM Journal on Scientific Computing, **31**, 890–912.

———, 2011, Sparse Optimization with Least-Squares Constraints: SIAM Journal on Optimization, **21**, 1201–1229.

Yu, Z., R. Abma, J. Etgen, and C. Sullivan, 2017, Attenuation of noise and simultaneous source interference using wavelet denoising: Geophysics, **82**, V179–V190.

Yu, Z., Z. Liu, G. Zhan, P. Cheng, B. Wang, and W. Fei, 2022, DAS noise attenuation using wavelet stack: Second International Meeting for Applied Geoscience & Energy, Society of Exploration Geophysicists and American Association of Petroleum Geologists, 592–596.

LIST OF FIGURES

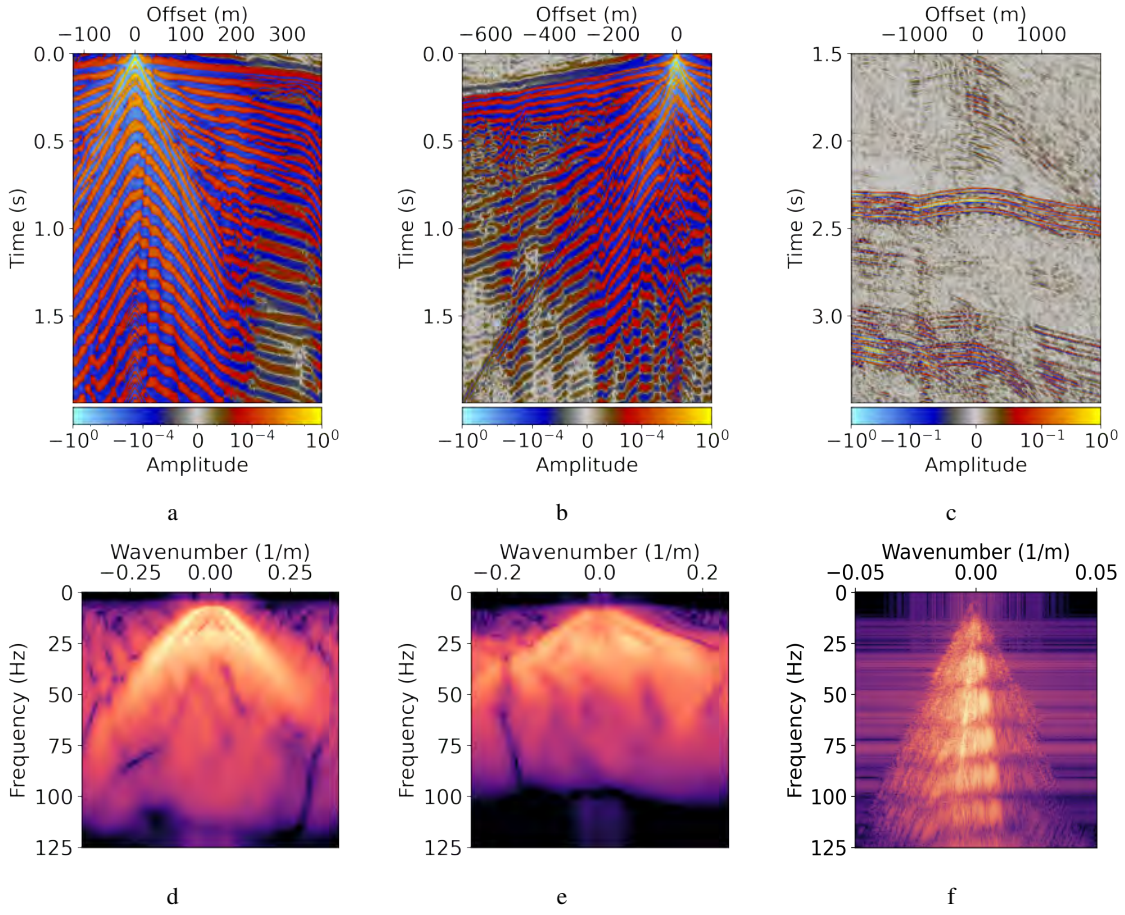

Figure 1: (a)-(c): Seismic records used for reconstructions experiments and (d)-(f) the corresponding FK spectra. (a) Land record with 1.25 m receiver spacing, (b) land record with 2 m receiver spacing, and (c) synthetic data with 10 m receiver spacing. All records are normalized such that their peak amplitude is 1. We use symmetric logarithmic scale to emphasize the large data dynamic range. FK spectra are displayed with logarithmic color mapping.
– **CWP-1017**

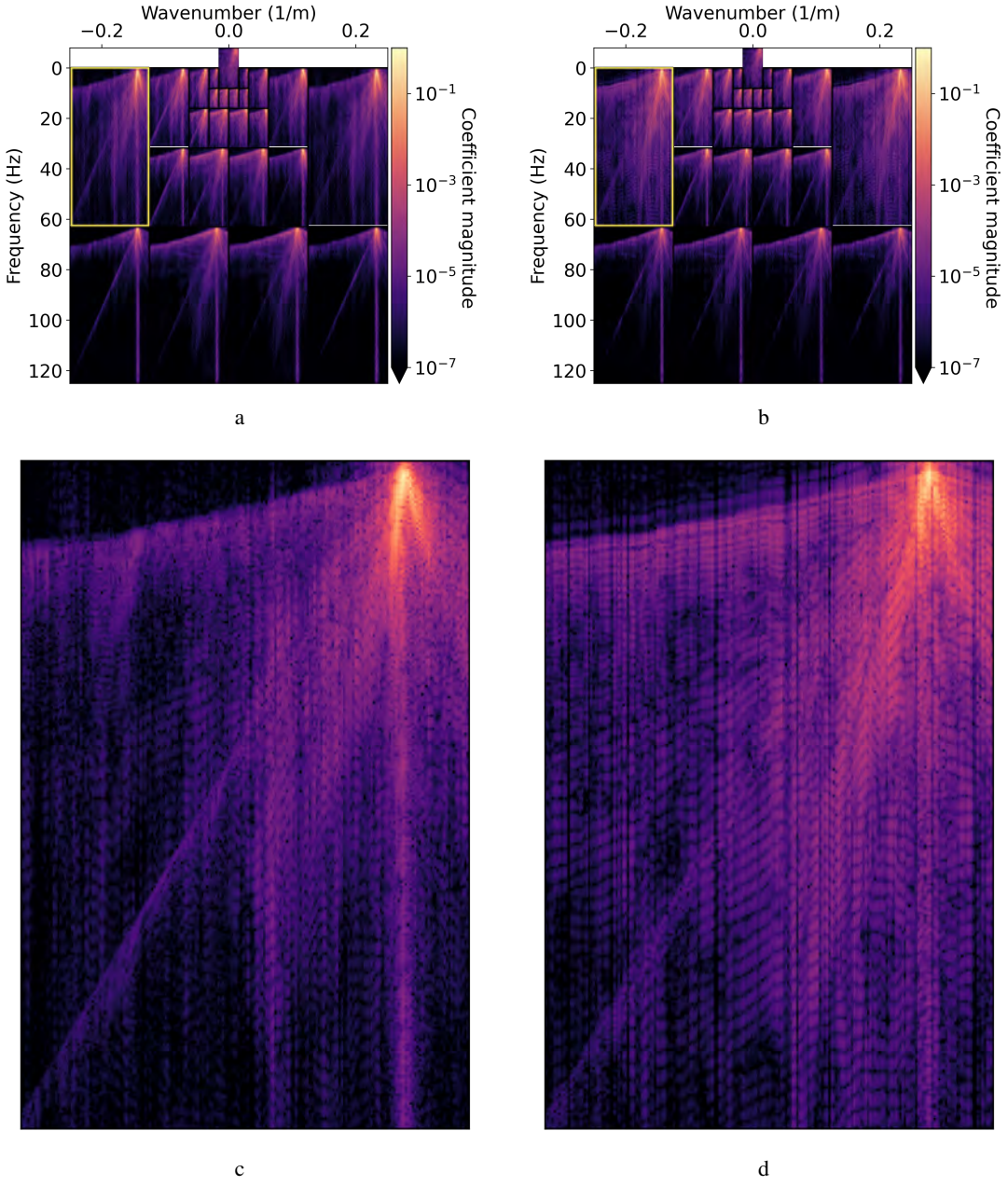

Figure 2: Magnitudes of complex wavelet coefficients for wavefield in Figure 1b: (a) before and (b) after random trace decimation. (c) and (d) are zoom on the $\mathbb{C}$WT coefficient magnitudes from yellow boxes in (a) and (b). Random trace decimation introduces stripe-like pattern mimicking missing trace geometry while the coefficients representing the remaining traces are strengthened.
– **CWP-1017**

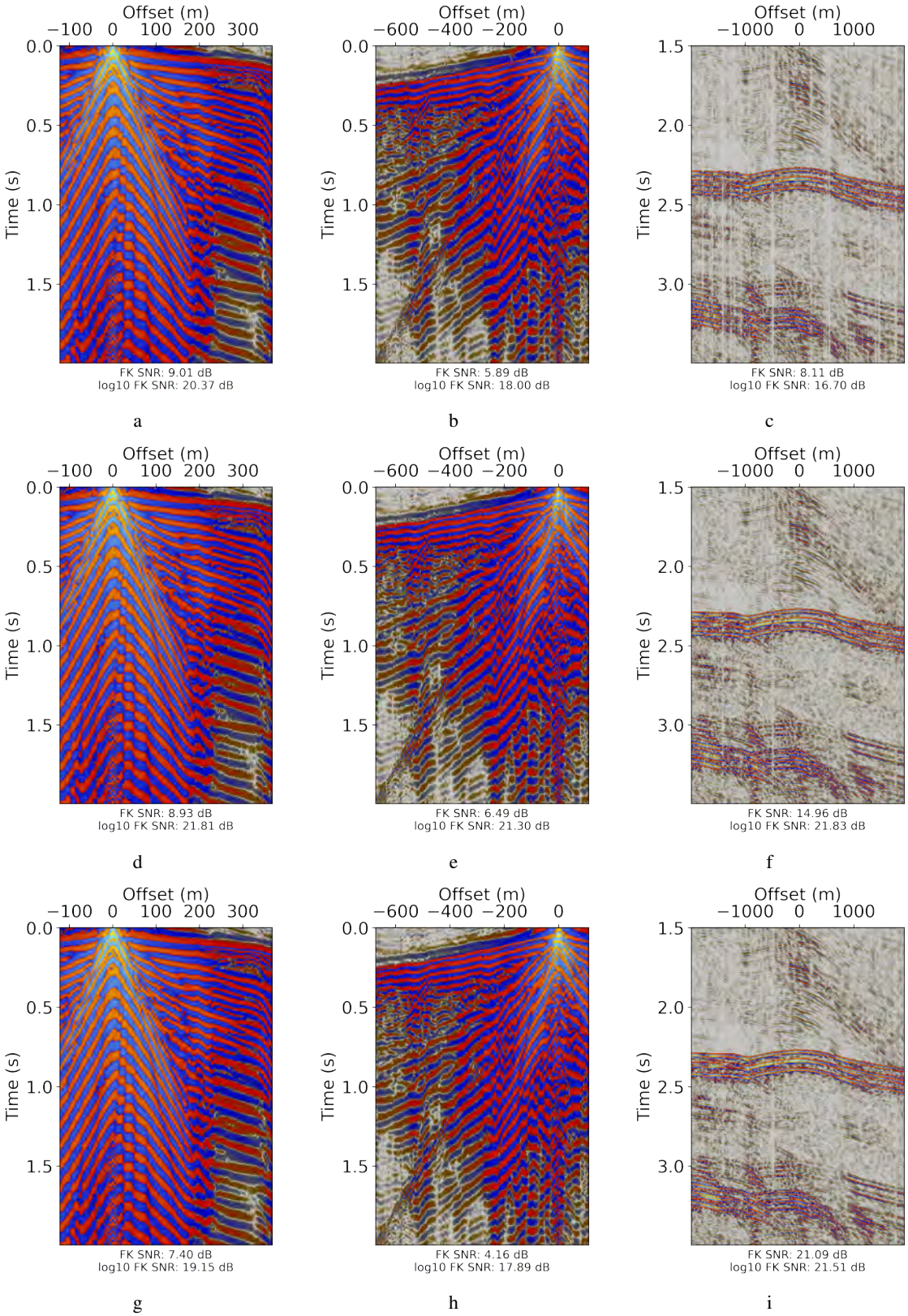

Figure 3: Reconstructions of the wavefields in Figure 1: (a)-(c) basis pursuit with SPGL1 solver, (d)-(f) iterative soft thresholding, and (g)-(i) POCS.

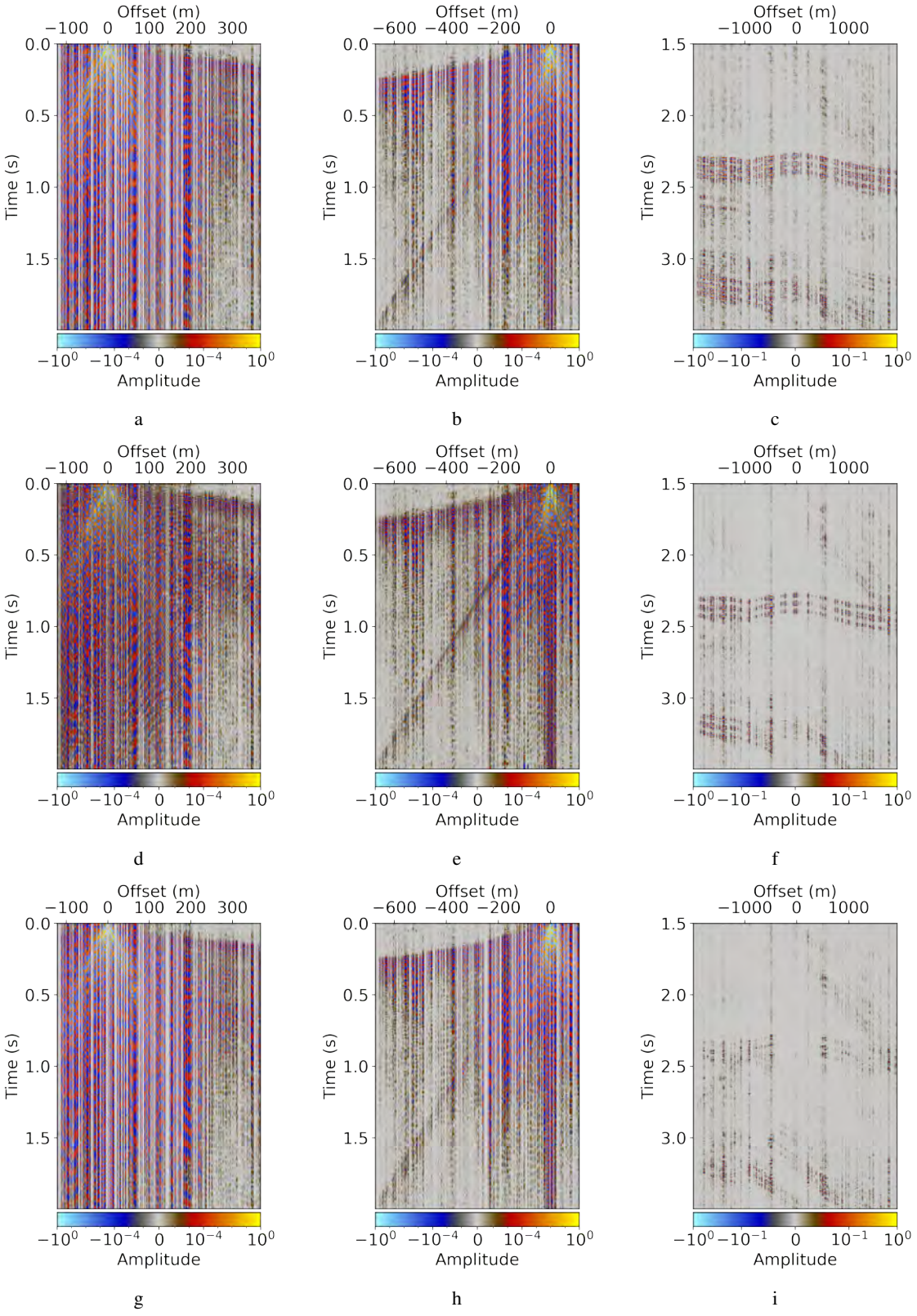

Figure 4: Data differences between fully sampled wavefields from Figure 1 and their reconstructions from Figure 3: (a)-(c) basis pursuit with SPGL1 solver, (d)-(f) iterative soft thresholding, and (g)-(i) POCS.